

Review

# 3D Porous MXene Films for Advanced Electromagnetic Interference Shielding and Capacitive Storage

Haoxiang Ma <sup>1</sup>, Changzheng Li <sup>1</sup> , Yang Yang <sup>1,\*</sup> and Zhimin Fan <sup>2,\*</sup> 

<sup>1</sup> Deep Sea Engineering Division, Institute of Deep Sea Science and Engineering, Chinese Academy of Sciences, Sanya 572000, China; mahx@idsse.ac.cn (H.M.); licz@idsse.ac.cn (C.L.)

<sup>2</sup> MIIT Key Laboratory of Critical Materials Technology for New Energy Conversion and Storage, School of Chemistry and Chemical Engineering, Harbin Institute of Technology, Harbin 150001, China

\* Correspondence: yangyang@idsse.ac.cn (Y.Y.); fanzm@hit.edu.cn (Z.F.)

**Abstract:** The construction of abundant pore channels between the layers of  $Ti_3C_2T_x$  MXene film is an important approach to fully exploit the 2D macromolecular properties of MXene ( $Ti_3C_2T_x$ ), which is of great significance for further realizing the practical application of MXene macroscopic assemblies in the field of electromagnetic interference shielding and capacitive storage. However, there is still a lack of systematic introductions and prospects of this field, thus far. In this review, starting from the preparation of MXene macroscopic assemblies, the 3D porous MXene films, constructed by sacrificial templating, vapor foaming, and light foaming, as well as their corresponding properties of electromagnetic interference shielding and capacitive storage, are introduced. In addition, the current bottlenecks and great challenges of 3D porous MXene films are deeply analyzed, and effective solutions for future application development trends are proposed.

**Keywords:**  $Ti_3C_2T_x$  MXene; porous structure; film; electromagnetic interference shielding; capacitive storage



**Citation:** Ma, H.; Li, C.; Yang, Y.; Fan, Z. 3D Porous MXene Films for Advanced Electromagnetic Interference Shielding and Capacitive Storage. *Crystals* **2022**, *12*, 780. <https://doi.org/10.3390/cryst12060780>

Academic Editor: Zhi Lin

Received: 7 May 2022

Accepted: 24 May 2022

Published: 27 May 2022

**Publisher's Note:** MDPI stays neutral with regard to jurisdictional claims in published maps and institutional affiliations.



**Copyright:** © 2022 by the authors. Licensee MDPI, Basel, Switzerland. This article is an open access article distributed under the terms and conditions of the Creative Commons Attribution (CC BY) license (<https://creativecommons.org/licenses/by/4.0/>).

## 1. Introduction

Since the discovery of graphene in 2004, two-dimensional (2D) materials have become the most dazzling star material in the 21st century. Such 2D materials have unique physical and chemical properties that ordinary materials do not have, thus bringing unlimited imagination to scientists and engineers. Especially in 2011, scientists from Drexel University synthesized a new type of 2D material called MXenes [1], which triggered a research upsurge in related fields. Different from the vast majority of 2D materials currently known, MXenes have high electrical conductivity, high hydrophilicity, and excellent processability, so they are widely used in energy storage [2,3], electromagnetic interference (EMI) shielding [4–8], biomedicine [9], sensor [10], communication [11], photothermal conversion [12], actuator [13–15], nanocomposite [16–18], and many other fields.

MXenes include 2D-transition metal carbides, nitrides, and carbonitrides, with the general chemical formula  $M_{n+1}X_nT_x$ , where M is an early transition metal (Ti, V, Nb, Mo, etc.), X represents C and/or N, and  $T_x$  stands for terminal surface groups (–OH, –F, and –O). At present,  $Ti_3C_2T_x$  MXene is the most studied and has the most comprehensive properties [19]. MXene ( $Ti_3C_2T_x$ ) has ultrahigh electrical conductivity ( $20,000\text{ S cm}^{-1}$ ) [20], which makes it quite useful in EMI shielding and electrochemical energy storage conversion. However, due to the strong van der Waals force and hydrogen bond between MXene layers, they will face the problem of serious aggregation between layers, when MXene layers are assembled into macro structures, which is unfavorable to the exposure of more active sites and the rapid transport of electrolyte ions. In addition, current aerospace EMI shielding materials are developing in the direction of lightweight, and due to the high density of MXene [21,22], its many macro-compact assemblies, obviously, cannot meet the above requirements. Accordingly, introducing pores between 2D MXene layers and,

then, assembling them into three-dimensional (3D) structure is an effective approach to settle the above problems [23–25]. On the one hand, the introduction of interlayer pores makes the MXene nanosheets have more interfaces, which can increase the propagation path of electromagnetic waves and, effectively, attenuate electromagnetic waves. On the other hand, the introduction of pore structure can significantly improve the transport kinetics of electrolyte ions, which, in turn, can effectively improve the capacitance and rate performance of MXene. Although there are some recent reviews on MXene foams and MXene aerogels, there are few reviews on porous MXene films that integrate porous and film-like structures.

This review, briefly, introduces the preparation of 3D porous MXene films by ice template, sacrificial template, vapor foaming, and light foaming methods, and focuses on the research progress of these 3D porous MXene films, for EMI shielding and electrochemical capacitive storage applications. In addition, the future development direction and trend of 3D porous MXene films are prospected.

## 2. 3D Porous MXene Films and Their EMI Shielding and Electrochemical Capacitance Properties

### 2.1. Preparation of MXene

In 2011, Gogotsi's students Naguib et al. [1] threw the  $Ti_3AlC_2$  MAX phase into HF and, successfully, produced a new 2D material called MXene. In fact, their original purpose was not to deliberately synthesize a 2D material, but to expand the space of the MAX phase to facilitate lithium intercalation/deintercalation [26]. As shown in Figure 1a, the morphology of  $Ti_3AlC_2$ , after being etched by HF, is accordion-like, and the obtained product is called multi-layer MXene, and its layers are mainly bonded by hydrogen bonds and van der Waals bonds. Such multi-layer MXene can be separated into delaminated MXene nanosheets by exfoliation methods, such as ultrasound (Figure 1b), but the yields are low and defects such as nanosheet-structure damage and oxidation are caused. Furthermore, some macromolecules, such as DMSO, can, spontaneously, intercalate between the multi-layer MXene layers to weaken the interlayer force [27], but this method is complicated and the effect is not ideal.

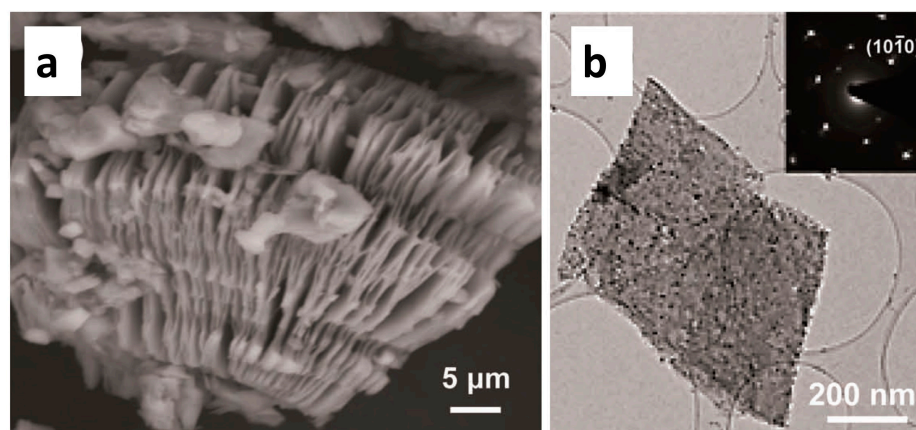


**Figure 1.** (a) SEM image of multi-layered  $Ti_3C_2T_x$  MXene. (b) TEM image of delaminated  $Ti_3C_2T_x$  MXene nanosheets; reproduced from [1], with the permission of Wiley-VCH.

To avoid the use of highly corrosive and highly toxic HF, Ghidui et al. [28], successfully, etched off the Al layer in  $Ti_3AlC_2$  using a mixed solution of LiF and HCl, so, then, individual MXene nanosheets can be easily obtained by ultrasonic stripping. In this process, the HF generated in situ by HCl and LiF can, effectively etch the Al layer of  $Ti_3AlC_2$ , while  $Li^+$  can spontaneously intercalate and expand the generated multi-layer MXene interlayer, thus ensuring the successful preparation of individual MXene nanosheets. On this basis, the scientists developed a minimally intensive layer delamination (MILD) method, by adjusting the molar ratio of LiF to the MAX phase and the concentration of HCl [29,30].

This improved method can produce large-size MXene nanosheets, with high yield and less surface defects (Figure 2a). The emergence of the MILD method has brought MXene materials into a stage of rapid and vigorous development. However, the easy oxidation of MXene in its aqueous dispersion limits its practical use [31–33]. In response to this issue, Gogotsi et al. [20] added excess Al during the synthesis of  $Ti_3AlC_2$  MAX phase, which can improve the crystallinity of  $Ti_3AlC_2$  grains and the stoichiometric ratio of carbon. The MXene prepared with this  $Ti_3AlC_2$  (Al- $Ti_3AlC_2$ ) as a precursor has high oxidation resistance, and the corresponding MXene dispersions can be stored for 10 months without obvious deterioration (Figure 2b). In addition to the HF etching and the in situ generation of HF to prepare MXene, there are, currently, methods such as fluorine-free etching, ammonium bifluoride etching, and the molten salt method [26]. It is worth noting that in all of these methods, the MILD method is a preparation method that can potentially scale up MXene from laboratory scale to commercial scale [34,35] (Figure 2c,d).

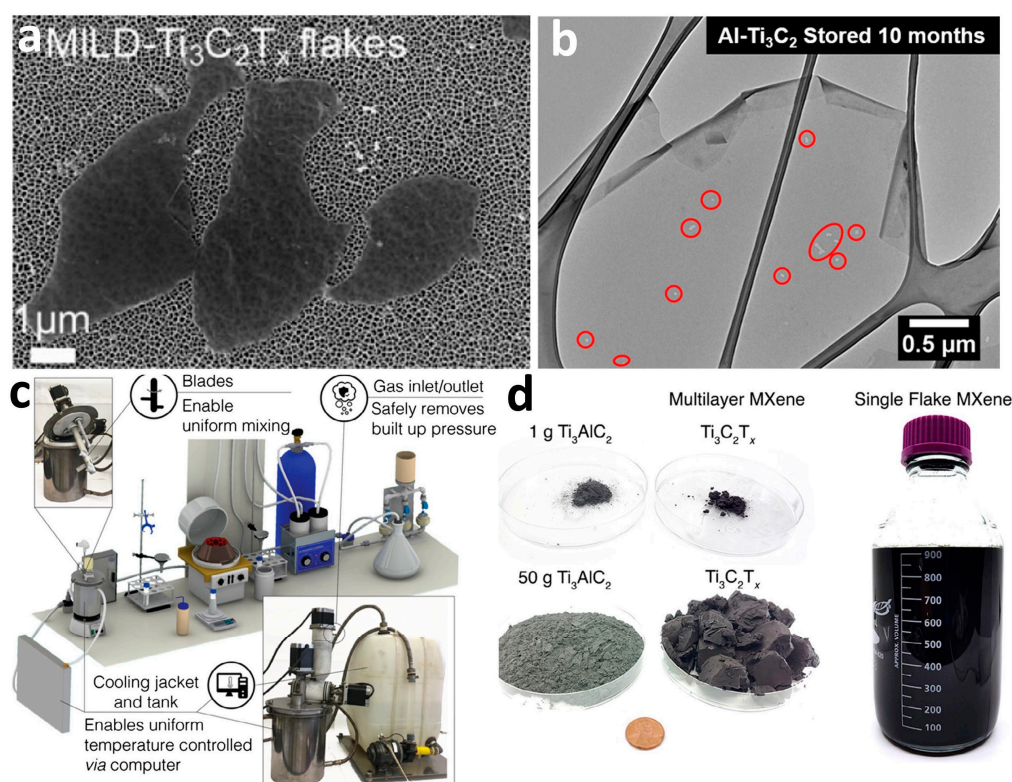


**Figure 2.** (a) SEM image of MILD- $Ti_3C_2T_x$  flakes; reproduced from [29], with the permission of the American Chemical Society. (b) TEM image of Al- $Ti_3C_2$  stored for 10 months; reproduced from [20], with the permission of the American Chemical Society. (c) Schematic of MXene scalable synthesis. (d) Comparison of small and large batches of synthesized MXene; reproduced from [34], with the permission of Wiley-VCH.

## 2.2. MXene Film and Its Properties

Assembly of individual MXene nanosheets into macrostructures is an essential process for their practical applications. Since MXene has a 2D macromolecular conformation similar to that of graphene oxide [36], MXene nanosheets are easily stacked to form thin films relying on interlayer van der Waals forces and hydrogen bonding. MXene films have extremely excellent electrical conductivity and high mechanical properties. Therefore, MXene films have been rapidly developed in the fields of EMI shielding and electrochemical capacitive storage. For example, the EMI shielding effectiveness (EMI SE) of a 45  $\mu\text{m}$ -thick MXene film in the X-band (8.2–12.4 GHz) is as high as 92 dB, which can effectively shield 99.9999994% of incident electromagnetic waves [5]. The main reason for the excellent EMI shielding ability of MXene film is due to the combined effect of its ultra-high electrical

conductivity and layered structural properties. The interface between the air and the highly conductive MXene film, with abundant free electrons on the surface, is in a high impedance mismatch (Figure 3a), so most of the electromagnetic waves will be reflected immediately, when the electromagnetic wave is incident on the surface of the MXene film. The residual electromagnetic waves can interact with the high electron density MXene and induce eddy currents when passing through the first layer of the MXene lattice structure, resulting in ohmic losses and a sharp attenuation of the electromagnetic wave energy. Importantly, the MXene film is composed of a stack of countless layers of MXene nanosheets, thus, there are countless processes of attenuating electromagnetic waves that are the same as the first layer of the MXene lattice. Meanwhile, the electromagnetic wave will, also, undergo multiple internal reflections between the layers of the MXene film, which can, also, effectively attenuate the electromagnetic wave entering the interior of the MXene film. In addition, local dipoles are generated between the Ti atoms on the terminal surface of MXene ( $\text{Ti}_3\text{C}_2\text{T}_x$ ) and the terminal groups, which can further attenuate electromagnetic waves. Combining the above factors, MXene films exhibit excellent EMI shielding ability, becoming one of the most excellent EMI shielding materials among known synthetic materials. Due to the compact stacked structure of MXene film, its density can be as high as  $4 \text{ g cm}^{-3}$ , which is not conducive to the demand of EMI shielding materials in the aerospace field, where lightweight is required. Therefore, it is of great significance to construct rich-pore structures in dense MXene films to obtain lightweight MXene films. More importantly, the introduction of the pore structure can increase more interfaces that interact with electromagnetic waves (Figure 3b), thus resulting in more excellent electromagnetic wave attenuation capabilities. Note that the MXene film relies on its intercalation pseudocapacitance in acidic electrolytes [37–41] and high density; therefore, its volumetric capacitance can be as high as  $1500 \text{ F cm}^{-3}$  [21].

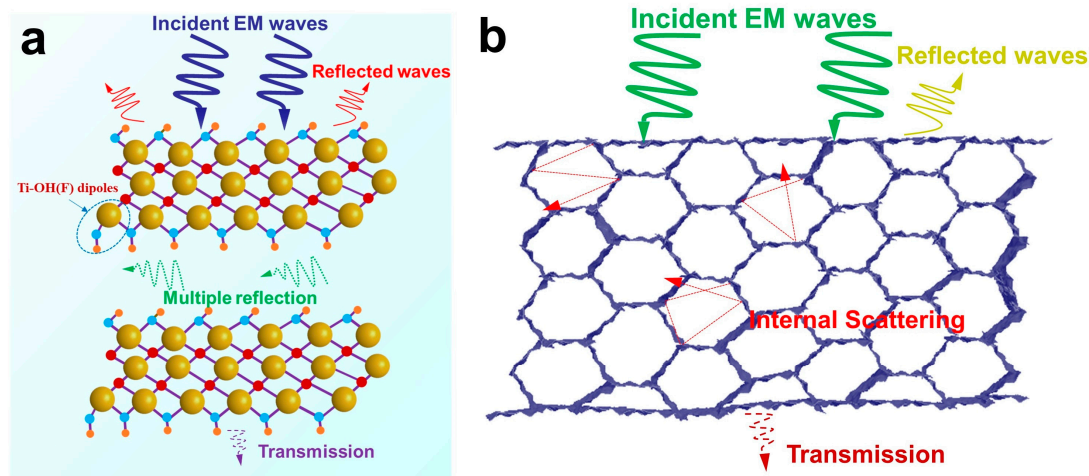


**Figure 3.** Schematic illustration of the electromagnetic waves transfer across the (a) MXene film and (b) 3D porous MXene film.

Commonly used preparation methods for MXene films include vacuum-assisted filtration, blade coating, and drop coating. Vacuum-assisted filtration is a method in which MXene nanosheets are separated from the corresponding solvent, using a vacuum pump and a filter membrane. At present, the commonly used method for preparing MXene films in the laboratory is mainly vacuum-assisted filtration, which is widely used because of its simple operation. However, the vacuum-assisted filtration method can only be used to produce small-sized MXene films, due to the limitation of the size of the filtration equipment. Moreover, because this method is energy-intensive and inefficient, it usually takes hours to prepare a piece of MXene film [42]. Note that the blade-coating method can process large-scale MXene films using industrially mature processes [22]. This method is not limited by the size of the equipment, and has the advantages of high efficiency and

continuous operation. Importantly, the MXene nanosheets can be oriented and arranged more regularly during the blade coating process; therefore, this MXene film has higher density and excellent mechanical properties. The drop-coating method is, also, a simple and efficient method to prepare MXene films. Lipton et al. [43] prepared MXene films, by dripping MXene dispersions on hydrophobic substrates. Since the interaction between the MXene nanosheets is stronger than the interaction between the MXene nanosheets and the substrate, the MXene film is easily peeled off from the substrate.

In addition to the conventional high conductivity and hydrophilicity, our research group [44] has recently discovered that MXene films can rely on water-assisted welding. Under the excitation of water droplets, the free water in the MXene film will re-diffuse and redistribute between layers, which can achieve a welding process similar to that of metals and plastics. Importantly, the welding of MXene films has a time-sensitive characteristic, that is, a free welding connection is possible during the time-sensitive period, and the weldability is lost outside the time-sensitive period. The weldability of MXene films enables the construction of complex multiscale structures such as common engineering materials. However, the disadvantages of MXene films with high density and a lack of continuous pores between layers limit their application in EMI shielding materials and high-rate electrochemical capacitive storage. Therefore, the development of a series of MXene films with rich interlayer porous structures is of great significance to promote the development of MXene materials.

### 2.3. Construction of 3D Porous MXene Films

#### 2.3.1. Ice Template Method

Whether it is HF etching or in situ generation of HF to prepare MXene, these methods belong to wet etching, so the macrostructure assembly of MXene is processed by MXene dispersion as raw material. That is to say, ice crystals can be used as sacrificial templates to construct 3D MXene foams or aerogels. For example, Bian et al. [25] used ice crystals as sacrificial templates to fabricate lightweight 3D MXene foams ( $10 \text{ mg cm}^{-3}$ ), with EMI shielding efficiencies (SE) and specific shielding efficiencies (SSE, SE per unit density) value as high as 75 dB and  $9904 \text{ dB cm}^3 \text{ g}^{-1}$ , respectively. It is worth noting that a certain amount of water molecules will remain between the layers of the MXene film, formed by MXene nanosheets stacked layer by layer, which creates an excellent ice-crystal-sacrificial-template medium between the MXene layers. Zhang et al. [45] filtered the MXene dispersion on a filter membrane to acquire a filter cake, which was then rapidly frozen in liquid nitrogen and freeze-dried to obtain a 3D macroporous MXene film with abundant interlayers (Figure 4a). During the rapid freezing process, the rapid growth of ice crystals leads to a significant expansion of the interlayers of the MXene films (Figure 4b). This 3D macroporous MXene film exhibits excellent specific capacitance and rate capability, and the assembled symmetric supercapacitor can achieve a capacitance retention rate of 87% after 4000 cycles (Figure 4c).

Direct filtration of MXene dispersions on membranes is inefficient and energy-intensive, and the face-to-face arrangement between MXene nanosheets results in limited space for expansion and contraction of ice crystals for growth. That is to say, there are a lot of closed dead spaces in the interlayer pores of the above-mentioned 3D macroporous MXene films, which is the main reason why the rate performance and cycle life improvement of such porous MXene films are limited. Based on this, our research group [46] utilizes monovalent metal ions to induce the aggregation of MXene nanosheets to form microgels, which can not only significantly improve the preparation efficiency of film hydrogels but also introduce continuous micro-nano pores between the nanosheets (Figure 5a). During the rapid freezing process, the continuous stretchable micro-nano pores provide a convenient channel for the free growth of ice crystals, so a 3D cellular MXene film with a continuous macropore structure can be obtained by freeze-drying (Figure 5b).

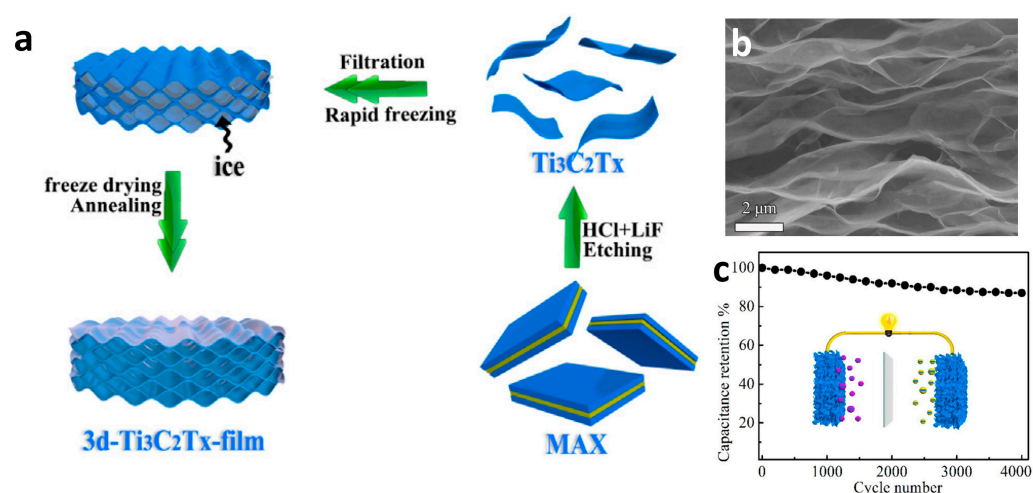


**Figure 4.** (a) Schematic of the preparation process of 3D  $Ti_3C_2T_x$  film. (b) Cross-sectional SEM image of 3D  $Ti_3C_2T_x$  film. (c) Prolonged cycling performance of the 3D  $Ti_3C_2T_x$  film-based symmetric supercapacitor at  $2 A g^{-1}$ ; reproduced from [45], with the permission of Elsevier.

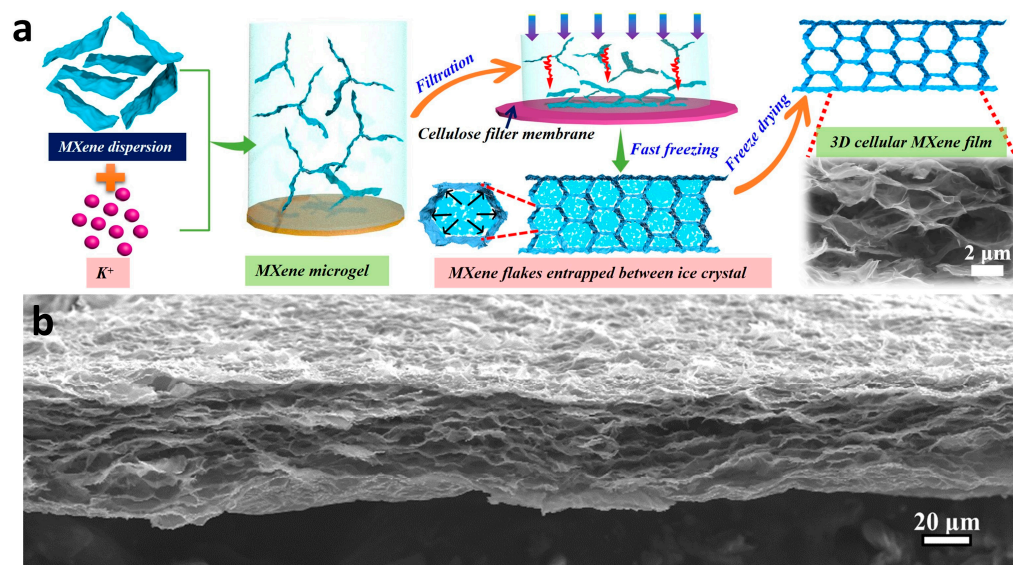


**Figure 5.** (a) Schematic of the preparation process of 3D cellular MXene film. (b) Cross-sectional SEM image of 3D cellular MXene film; reproduced from [46], with the permission of the American Chemical Society.

Based on unique continuous pore channels, high electrical conductivity, and excellent mechanical properties, the specific capacitance of 3D cellular MXene film is significantly better than that of MXene film, and the capacitance retention rate is 76% at scan rates as high as  $200 mV s^{-1}$  (Figure 6a), exhibiting excellent rate performance. Since the structural framework of the 3D cellular MXene film is composed of lapped and expanded MXene microgels, more active sites for pseudocapacitive reactions can be exposed. Furthermore, even during rapid charge and discharge, the electrolyte ions can pass through the 3D continuous pore channels, so that 99.8% of the initial capacitance can still be retained after 10,000 cycles (Figure 6b), showing an extremely excellent cycle life. The 3D cellular MXene film has continuous macropores between the layers, and its density is reduced to  $0.23 g cm^{-3}$  compared to the pure MXene film ( $3.9 g cm^{-3}$ ), so it has a significant role in the field of lightweight EMI shielding materials for aerospace. As shown in Figure 6c, the average EMI SE value of the 3D cellular MXene film with a thickness of  $86 \mu m$  can be as high as 78 dB, which means that 99.99999% of the incident radiation can be blocked, showing extremely excellent EMI shielding performance.

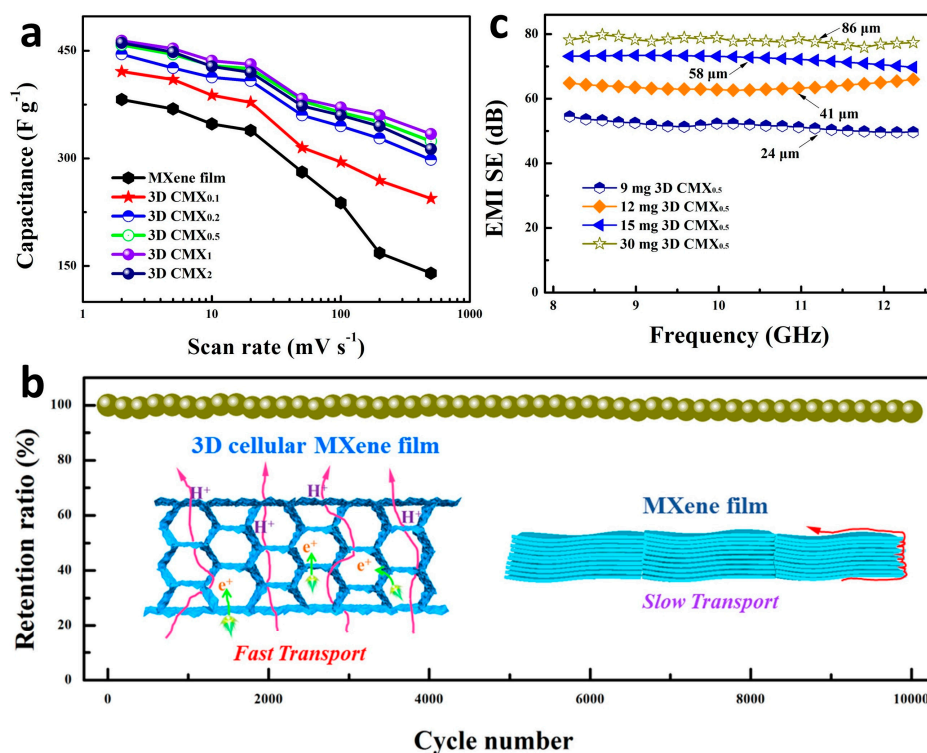


**Figure 6.** (a) Capacitances of 3D cellular MXene film at different scan rates. (b) Prolonged cycling performance of 3D cellular MXene film at 100 mV s<sup>-1</sup>. (c) EMI SE of the 3D cellular MXene film with different thicknesses; reproduced from [46], with the permission of the American Chemical Society.

Similarly, Kong et al. [47] obtained a high-mass-loading 3D porous MXene film with ultrahigh-rate pseudocapacitive properties, by freeze-casting using ice crystals as templates. As shown in Figure 7a, the addition of KOH solution to the MXene dispersion resulted in the formation of an electric double layer on the MXene surface and shielded the surface charges to weaken the electronegativity of functional groups, thereby reducing the electrostatic repulsion of the MXene nanosheets and forming flocs. The free-standing 3D porous MXene film were then obtained by freeze casting. The existence of macroporous structure can make ions more accessible and easier to diffuse on the surface of MXene. Based on this, the 3D porous MXene film can exhibit a specific capacitance of 358.8 F g<sup>-1</sup> at 20 mV s<sup>-1</sup>, which is significantly better than that of MXene film (Figure 7b). When the scan rate was increased to 10,000 mV s<sup>-1</sup>, the 3D porous MXene film could still maintain the shape of the CV curve well, with a capacitance retention of 58.6% and a 1000-fold increase in scan rate (Figure 7c). In addition, at a mass loading of 16.18 mg cm<sup>-2</sup>, the 3D porous MXene film can exhibit ultra-high areal capacitance (3731 mF cm<sup>-2</sup>) and high energy density (336.7 μWH cm<sup>-2</sup>). This means that such 3D porous MXene film can show excellent specific capacitance and high-rate performance, on the premise of meeting the actual mass loading (>10 mg cm<sup>-2</sup>), which is of great significance to promote the practical application of MXene materials in the field of electrochemical energy storage.

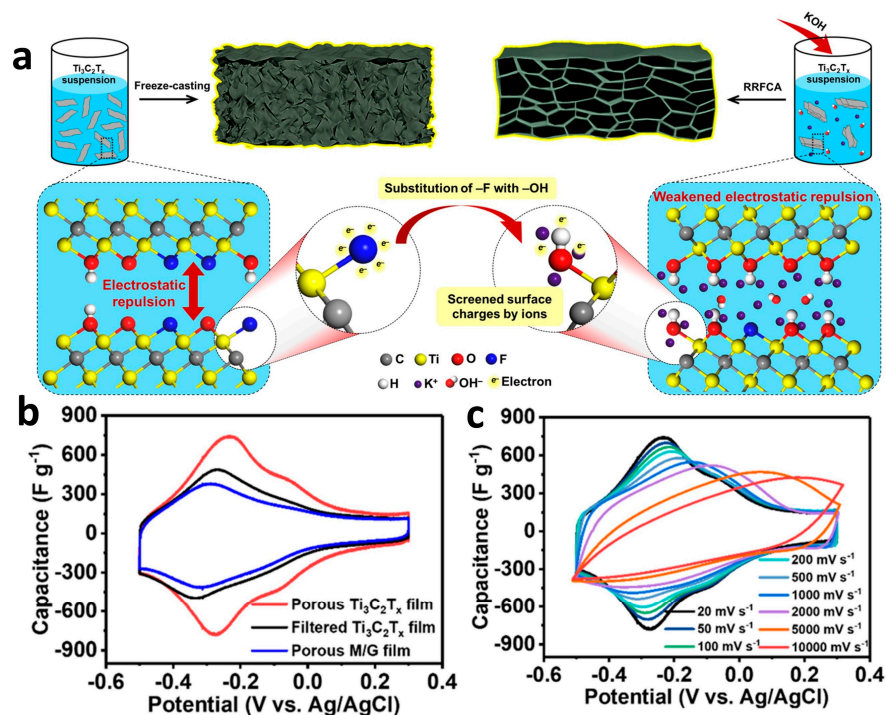


**Figure 7.** (a) Comparison of conventional freeze-casting and reduced-repulsion freeze-casting assembly processes. (b) CV curves of porous M/G film, filtered  $\text{Ti}_3\text{C}_2\text{T}_x$  film, and 3D porous  $\text{Ti}_3\text{C}_2\text{T}_x$  film at  $20 \text{ mV s}^{-1}$ . (c) CV curves of 3D porous  $\text{Ti}_3\text{C}_2\text{T}_x$  film at the different scan rates ranging from 20 to 10,000  $\text{mV s}^{-1}$ ; reproduced from [47], with the permission of the American Chemical Society.

To more significantly increase the exposure of MXene active sites, Zhang et al. [48] developed a simple in situ ice templating strategy to fabricate 3D porous MXene films. They introduced a small number of carbon nanotubes into MXene, in order to expand the interlayer spacing of MXene, so that more interlayer water can be converted into ice templates, which, in turn, can form a more developed porous structure after freeze-drying (Figure 8a). Since the 3D structure in MXene significantly increases the exposure of active sites on the surface of the MXene nanosheet and accelerates the migration of ions, the flexible 3D porous MXene film shows a specific capacitance of  $375 \text{ F g}^{-1}$  at  $5 \text{ mV s}^{-1}$ . At the same time, it can maintain an excellent capacitance retention rate of  $251.2 \text{ F g}^{-1}$  at  $1000 \text{ mV s}^{-1}$  (Figure 8b). In fact, the construction of 3D porous MXene films by the ice template method can, also, be regarded as a template-free preparation method, since they all use the aqueous dispersion of MXene as the pre-material. That is, no additional external water was introduced to construct the ice template during this process. Therefore, the preparation of 3D porous MXene films using ice templates is a green and energy-saving method, and it is easy to scale.

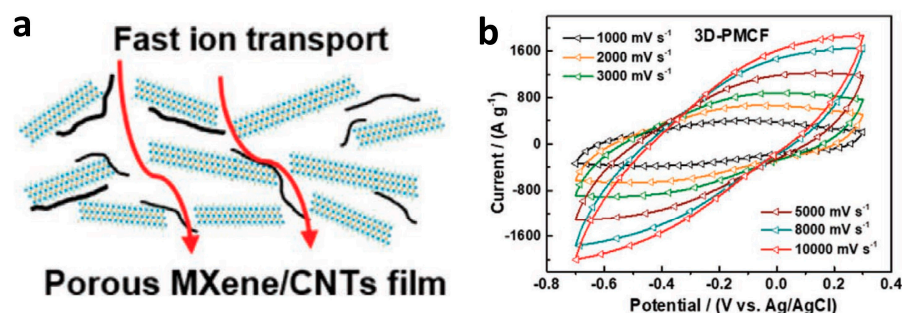


**Figure 8.** (a) Schematic illustration of ion diffusion pathways across the porous MXene/CNTs film. (b) CV curves of porous MXene/CNTs film at the different scan rates ranging from 1000 to 10,000  $\text{mV s}^{-1}$ ; reproduced from [48], with the permission of Wiley-VCH.

### 2.3.2. Sacrifice Template Method

In addition to ice crystals that can be used as sacrificial templates to construct 3D porous MXene films, some polymers can, also, play the same role, and can further improve the comprehensive properties of 3D porous MXene films during the calcination process. Zhao et al. [49] employed polymethyl methacrylate (PMMA) spheres as sacrificial templates, to successfully process MXene nanosheets into 3D macroporous MXene films, with hollow spherical structures between layers. As shown in Figure 9a, MXene nanosheets are, spontaneously, wrapped on the surface of PMMA spheres driven by their terminal active functional groups, and then the stacking density of PMMA/MXene composite microspheres can be increased by vacuum-assisted filtration, thereby constructing PMMA spheres/MXene composite films. Finally, 3D macroporous MXene films were obtained by calcining at 450 °C to remove the PMMA spheres. In fact, this 3D macroporous MXene film is an MXene–carbon hybrid foam material, but it still has excellent flexibility (Figure 9b). From the cross-sectional SEM image of the 3D macroporous MXene film (Figure 9c), it can be seen that the 3D macroporous MXene film is a 3D framework composed of a large number of MXene hollow spheres, which leads to a decrease in the film packing density, from  $3.8 \text{ g cm}^{-3}$  for dense film to  $0.4 \text{ g cm}^{-3}$  for macroporous film. This 3D macroporous MXene film can be directly used as the anode of Na-ion battery, without additional additives. At a charging rate of 0.25 C, the reversible capacity of the 3D macroporous MXene film can reach 330 mAh, with excellent rate performance and long-cycle stability. Interestingly, this 3D macroporous MXene film can, also, exhibit a high specific capacitance of  $210 \text{ F g}^{-1}$  at scan rates as high as  $10 \text{ V s}^{-1}$ , due to the continuity of the interlayer pores and sufficient exposure of the active surface, surpassing the best known carbon-based supercapacitors. Note that this 3D macroporous MXene film is more suitable as a material for EMI shielding, since its pore structure can be adjusted at will by adjusting the size of the sacrificial template, thereby making the material lighter with more loss of incident electromagnetic waves.

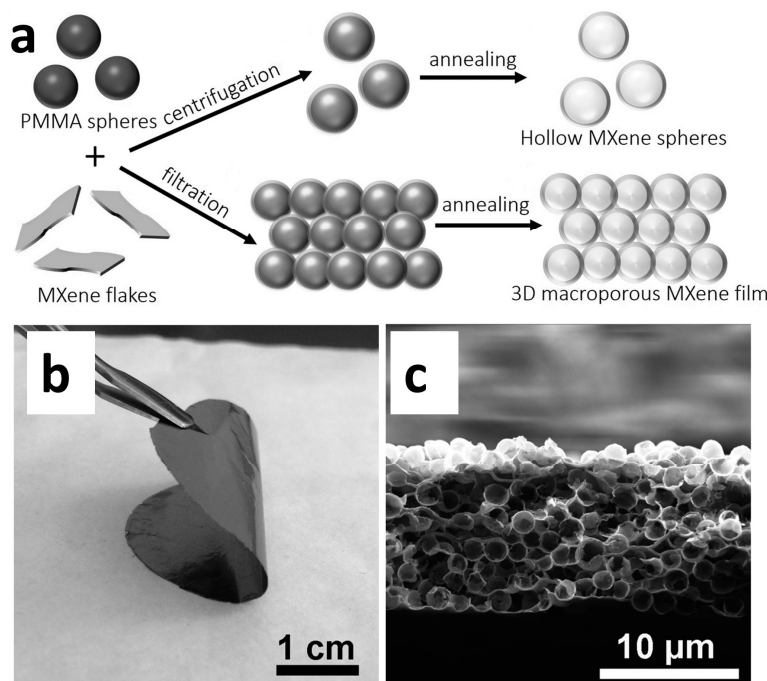


**Figure 9.** (a) Schematic diagram of synthesis of 3D macroporous MXene film. (b) Digital photograph showing the flexibility of 3D macroporous MXene film. (c) Cross-sectional SEM image of 3D macroporous MXene film; reproduced from [49], with the permission of Wiley-VCH.

Similar to the use of polymer sacrificial templates, Zhao et al. [50], also, constructed 3D porous MXene films using sulfur templates. As shown in Figure 10, sulfur particles are, first, generated by chemical reaction of sodium thiosulfate with excess HCl and polyvinylpyrrol-

done dispersant. It is worth noting that the synthesized sulfur particle size is controllable and has good dispersibility in water. Therefore, the sulfur particles can be uniformly distributed in the MXene dispersion, and, then, the MXene/sulfur particle composite film is obtained by vacuum-assisted filtration. Next, the sulfur particles were sublimed off under the protection of inert gas at a temperature of 300 °C, and a flexible 3D porous MXene film was obtained. This 3D porous MXene film is free-standing and, thus, can be directly used as electrodes for lithium-ion batteries. Since the porous structure in the 3D porous MXene film can provide a large number of active sites, the lithium storage capacity can be significantly improved. In addition, the continuous pore structure enables unimpeded transport of lithium ions. Based on the above advantages, the 3D porous MXene film can achieve a capacity of 455.5 mAh g<sup>-1</sup> at 50 mA g<sup>-1</sup> and exhibit extremely excellent ultra-long-term cycling stability. It is well known that doping graphene with heteroatoms is an important strategy to improve electrochemical capacitive properties. In fact, we can also use this sulfur-template-like approach to dope N and other heteroatoms into the MXene structure, to further enhance the electrochemical capacitive performance.

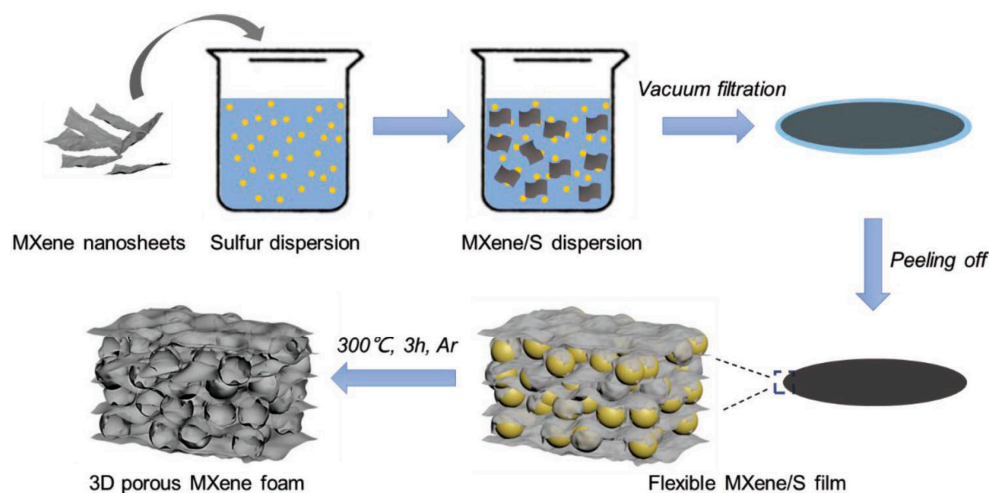


**Figure 10.** Schematic diagram of 3D porous MXene film synthesis using sacrificial sulfur template; reproduced from [50], with the permission of Wiley-VCH.

The interlayer pores of the above 3D MXene films are all large in size. Although the aggregation between the MXene nanosheets can be well suppressed and the active sites are fully exposed, most of the space of these large pores will be filled with electrolytes when used as electrodes. In fact, only the electrolyte in contact with the surface of the MXene nanosheet can contribute to the efficient electrochemical reaction, while the vast majority of electrolytes only increase the quality of the overall device, without any capacitive contribution. Therefore, our team [51] successfully constructed nanoporous MXene films with dense structure and interconnected nanopores channel between layers using a nanoscale sacrificial template (Figure 11). The size of Fe(OH)<sub>3</sub> nanoparticles is between 3 nm and 5 nm, and the surface is positively charged. Therefore, the negatively charged MXene colloidal dispersion and the positively charged Fe(OH)<sub>3</sub> colloidal nanoparticles form a homogeneous mixture by electrostatic self-assembly. Afterwards, nanoporous MXene films were obtained by vacuum-assisted filtration and etching of Fe(OH)<sub>3</sub> nanoparticles with HCl. To improve the electrochemical capacitance, this nanoporous MXene film was then subjected to appropriate heat treatment to obtain a modified nanoporous MXene film. This modified nanoporous MXene film has the same flexibility as pure MXene film, which can be bent at will. Importantly, the interlayer pores of the modified nanoporous MXene films are coherent and interconnected, thereby effectively promoting the rapid transport of ions without affecting the high density of the films. Based on this, the volumetric capacitance of the modified nanoporous MXene film at 0.5 A g<sup>-1</sup> is as high as 1142 F cm<sup>-3</sup>, and it has excellent rate capability. In addition, when the mass loading reaches the actual use

standard, it can, also, show an excellent volume specific capacitance. Therefore, we can tune and optimize the interlayer pore structure of 3D porous MXene films according to different usage scenarios. Large-scale pore structures should be introduced in EMI shielding applications requiring lightweight fields, while nano-scale pore structures should be introduced in compact portable electrochemical energy storage devices.

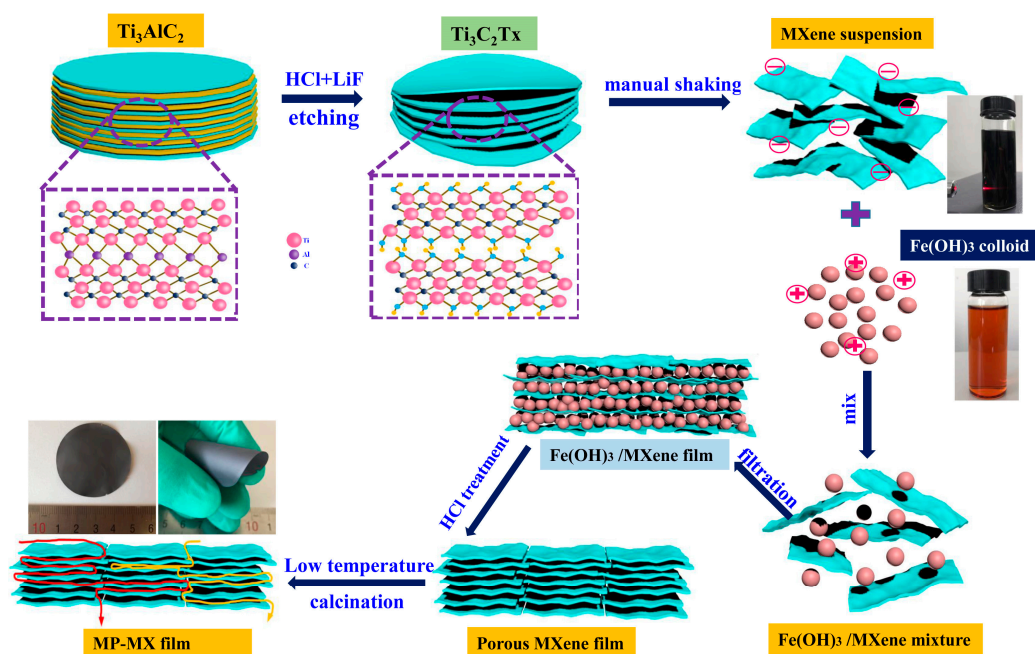


**Figure 11.** Schematic diagram of synthesis of nanoporous MXene film; reproduced from [51], with the permission of the Royal Society of Chemistry.

Similar to graphene, MXene is, also, a high-barrier 2D material [42]; therefore, electrolyte ions cannot pass through the MXene nanosheet across the plane, but can only pass through the next layer of MXene along the edge of the nanosheet. Although the above-mentioned 3D porous MXene films have abundant pore channels between the layers, the ion transport path is still tortuous. Tang et al. [52] used  $\text{H}_2\text{SO}_4$  oxidation to etch uniform nanopores in the MXene nanosheets, which not only significantly increased the number of active sites but also ions could directly enter the next layer of MXene along the nanopore channels, thereby greatly shortening the ion transport path (Figure 12a). When this MXene film with in-plane nanopores is used for supercapacitor electrodes, it can show extremely excellent rate capability and ultra-long cycling stability (Figure 12b). In fact, MXene with in-plane nanopores still have a serious tendency to aggregate when assembled into films. To further improve the ion transport kinetics, our group [53] used volatile and non-volatile liquids to precisely control the interlayers of MXene with in-plane pores, and obtained a dense porous MXene film with in-plane and interlayer coherent pores. This porous MXene film integrates high volumetric capacitance, excellent rate capability, and high mass loading, showing excellent ion transport kinetics (Figure 12c). Based on this, in the future, we can etch nanopores in the MXene nanosheet level, and, then, use a sacrificial template to construct a new type of 3D porous MXene film, which is bound to further enhance the competitiveness of MXene materials in the fields of EMI shielding and electrochemical capacitance storage.

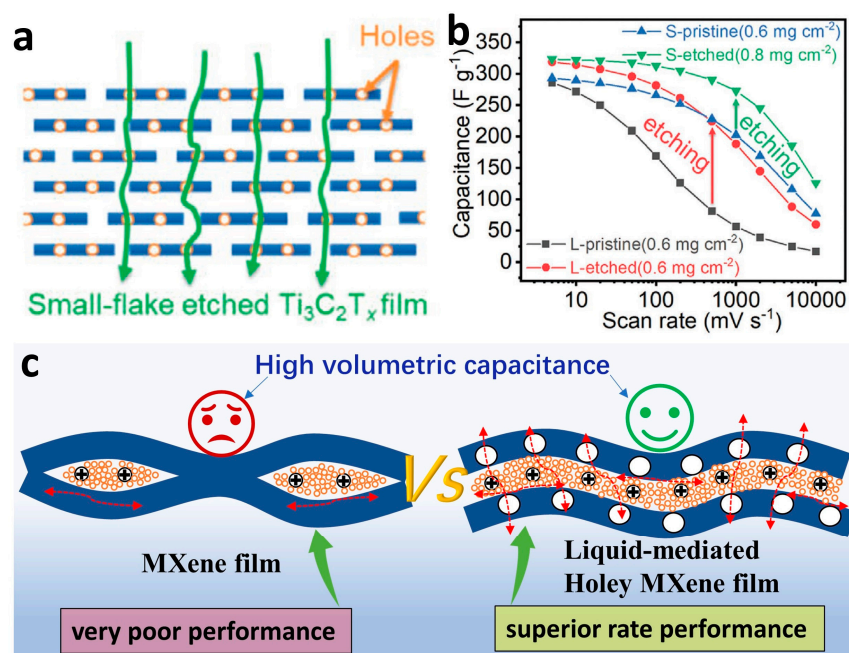


**Figure 12.** (a) Schematic illustration of ion diffusion pathways across the holey MXene film. (b) Capacitances of holey MXene film at different scan rates; reproduced from [52], with the permission of Wiley-VCH. (c) Schematic illustration of ion diffusion pathways across the liquid-mediated holey MXene film; reproduced from [53], with the permission of Elsevier.

### 2.3.3. Vapor Foaming

Although the template method can effectively build a pore structure between the MXene films, this method is cumbersome, due to the need to remove the template. In our daily diet, dough fermentation is an essential process, since the gas produced can make the (steamed) bread more fluffy and more suitable for people to chew. Inspired by this process, Niu et al. [54] utilized hydrazine hydrate to generate hydrazine vapor at high temperature and pressure, to induce interlayer foaming of dense graphene oxide films. As shown in Figure 13a, the graphene oxide nanosheets can be assembled into flexible graphene oxide films by vacuum-assisted filtration. Subsequently, the graphene oxide film was placed in a certain concentration of hydrazine hydrate and heated to 90 °C for 10 h. Since graphene oxide is very unstable, steam (from water) and  $CO_2$  are generated under the action of hydrazine hydrate reduction, which, in turn, induces the foaming of graphene oxide films into 3D porous graphene films. This 3D porous graphene film exhibits excellent capacitance–storage–conversion performance, when used in supercapacitors. Subsequently, Shen et al. [55], also, used the same method to construct a 3D porous graphene film. The existence of a large number of abundant pore interfaces can generate multiple reflections of electromagnetic waves inside the 3D porous graphene film, which can, effectively, attenuate electromagnetic waves. Similar to graphene oxide, the MXene terminal is rich in reactive functional groups such as  $-OH$ , so it can, also, be foamed with hydrazine vapor. Liu et al. [56] successfully foamed dense MXene films into a lightweight 3D porous MXene film using hydrazine vapor under high pressure (Figure 13b). It is worth noting that the amount of oxygen-containing functional groups at the MXene terminals is significantly reduced under the action of hydrazine vapor, which endows the 3D porous MXene films with excellent hydrophobic properties. Since conventional MXene face the risk of being easily oxidized in humid environments, this hydrophobic 3D porous MXene film effectively overcomes this problem. Based on high electrical conductivity and rich foam structure, this hydrophobic and lightweight 3D porous MXene film shows extremely excellent EMI shielding performance, and, thus, has important application value in the field of EMI shielding materials for aerospace.

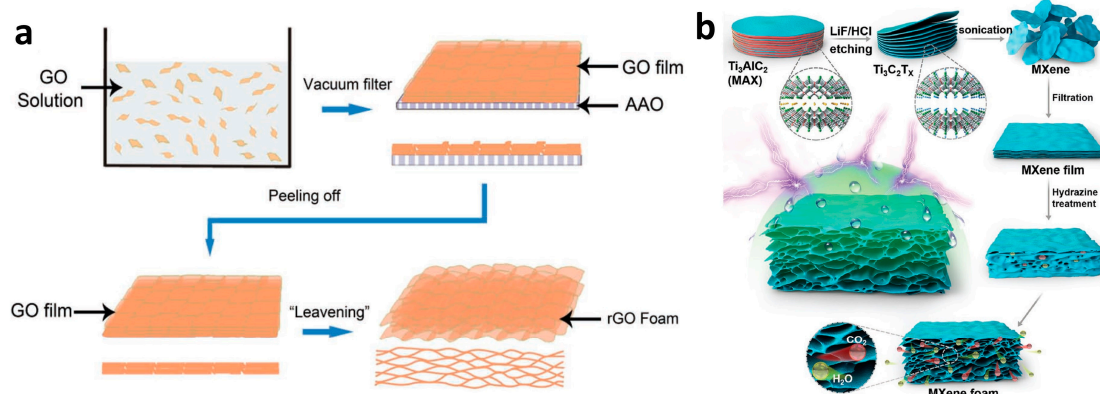


**Figure 13.** (a) Schematic illustration of the fabrication of the leavening process to prepare rGO foams; reproduced from [54], with the permission of Wiley-VCH. (b) Schematic diagram of the synthesis of the hydrophobic and flexible MXene foam; reproduced from [56], with the permission of Wiley-VCH.

Since MXene has a similar structure to graphene, Zhang et al. [57] were inspired by this to propose a new method for the assisted construction of 3D porous MXene films using graphene oxide (Figure 14). First, they obtained MXene/graphene oxide films by ion-induced mixed colloidal dispersion of MXene and graphene oxide, followed by vacuum-assisted filtration. Subsequently,  $HCO_3^-$  ions can be completely decomposed into  $CO_2$  and  $H_2O$  vapor during the stepwise reduction of graphene oxide by HI at high temperature, thus inducing foaming to obtain 3D porous MXene/graphene composite films. Due to the synergistic effect of high electrical conductivity and porous structure, the EMI shielding effectiveness value of this 3D porous MXene/graphene composite film can reach 59 dB, and the corresponding absolute EMI SE value can be as high as  $37,619 \text{ dB cm}^2 \text{ g}^{-1}$ . Importantly, this 3D porous MXene/graphene composite film has superior hydrophobicity, thus avoiding the risk of water oxidation. In addition, this foaming process can avoid the use of toxic hydrazine hydrate, thus showing environmental friendliness.

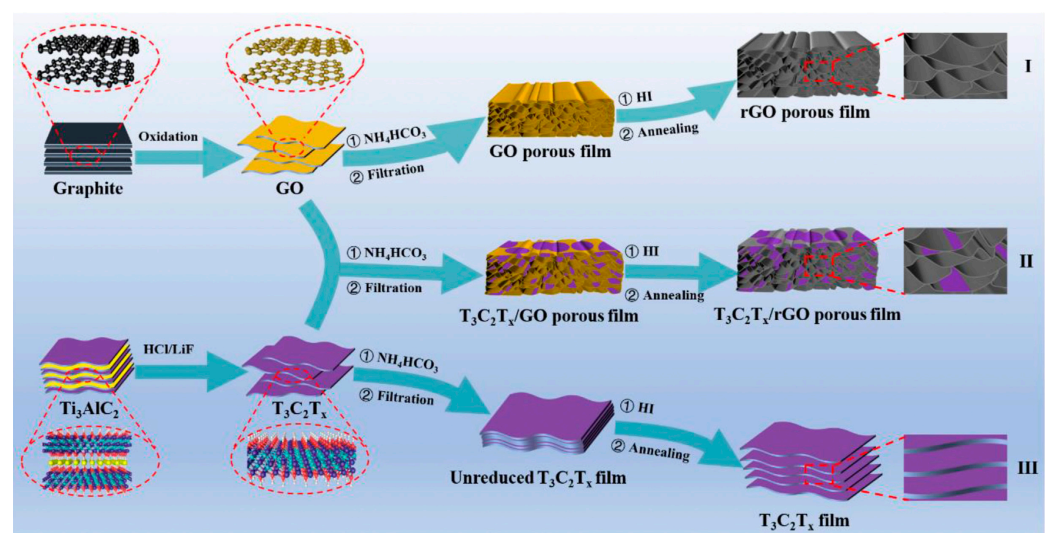


**Figure 14.** Schematic illustration of the fabrication of the  $Ti_3C_2T_x/rGO$  porous film; reproduced from [57], with the permission of Elsevier.

### 2.3.4. Light Foaming

It is well known that the excellent ability of MXene in electromagnetic wave absorption makes it a photothermal conversion material, with a conversion efficiency of almost 100%; therefore, MXene shows important application prospects in the fields of photothermal cancer therapy [58,59], seawater desalination [60], etc. A certain amount of water molecules

will remain between the layers of MXene films obtained by vacuum-assisted filtration or blade coating. In addition, the MXene terminal surface is, also, rich in a large number of oxygen-containing active functional groups. The high temperature instantaneously generated when the MXene film is exposed to light can vaporize the interlayer water and oxygen-containing functional groups, and, then, rapidly expand the MXene film to foam. Tang et al. [61] used a laser to inscribe the surface of the MXene film, to instantly photothermally vaporize the interlayer water and oxygen-containing functional groups on the terminal surface, successfully creating abundant pore channels (Figure 15). Since the stacked MXene nanosheets are converted into a 3D porous framework structure, the rate capability of the MXene films is significantly improved. In addition, the electrochemical performance can be well controlled, by adjusting the linear density of the laser scanning path. The microsymmetric supercapacitor assembled from the laser-scribed 3D porous MXene film exhibits a high areal capacitance of  $15.03 \text{ mF cm}^{-2}$  at  $10 \text{ mV s}^{-1}$ , while exhibiting ultra-high capacitance retention.

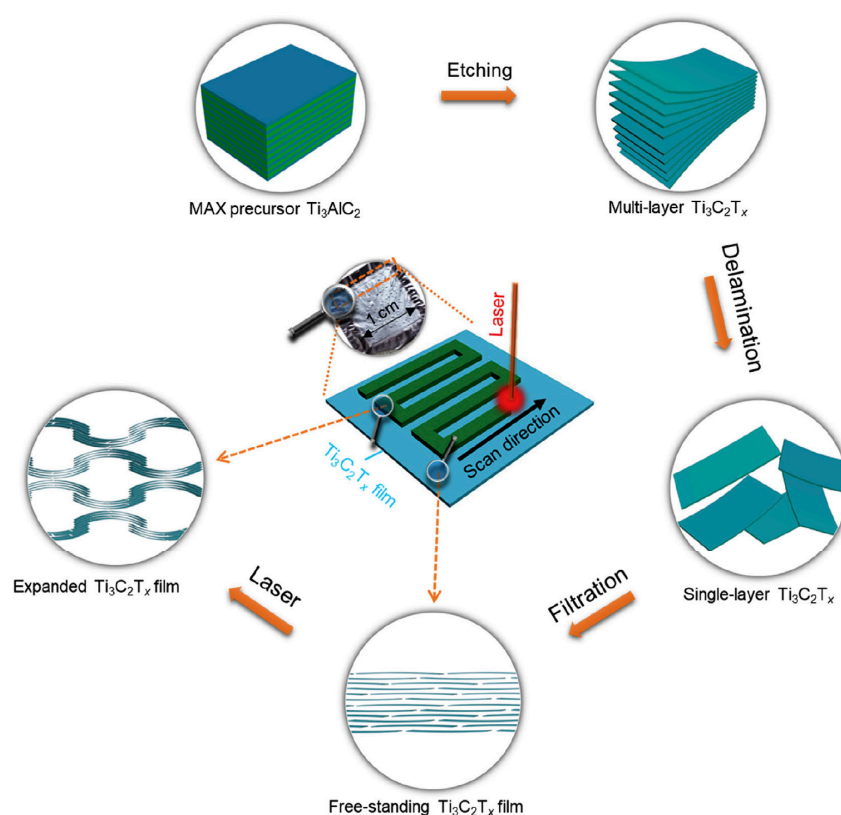


**Figure 15.** Schematic diagram of 3D porous MXene film synthesis using laser engraving; reproduced from [61], with the permission of Elsevier.

Sunlight is inexhaustible. If sunlight can be used in foamed MXene films, it will be of great significance to promote the practical application of MXene materials. Our research group [62] focused the sunlight to irradiate the MXene film, and realized the rapid foaming of the conventional dense MXene film (Figure 16a). The interlayer free water and oxygen-containing functional groups of the MXene film can be instantly vaporized by the photothermal effect induced by the focused sunlight, which, in turn, causes the MXene nanosheet to expand rapidly along the trans-planar direction. In addition, the force between the MXene nanosheets inhibits their unrestricted expansion, resulting in a 3D porous MXene film with interlayer-like honeycomb-like pores (Figure 16b). This 3D porous MXene film exhibits electrical conductivity up to  $1000 \text{ S cm}^{-1}$  and is lightweight as well as flexible. In addition, the 3D porous MXene film exhibited high hydrophobicity and environmental stability, due to the removal of a large number of oxygen-containing

functional groups, and the improvement of the surface roughness of the MXene films. Based on the continuous porous structure and more exposed active sites, this 3D porous MXene film exhibits high specific capacitance up to  $350 \text{ F g}^{-1}$  and excellent rate capability, making it attractive for high-rate energy storage applications. In addition, the absolute EMI SE value of a  $10 \text{ }\mu\text{m}$ -thick 3D porous MXene film can be as high as  $61,608 \text{ dB cm}^2 \text{ g}^{-1}$ , when used as an EMI shielding material (Figure 16c), showing a potential application in the field of EMI shielding materials for aerospace. Importantly, the sunlight-focused foamed MXene film can be completed in seconds, which is a high efficiency far from the template method and the vapor method. Therefore, the sunlight-focused foaming method has the advantages of simplicity, efficiency, environmental protection, low cost, and easy expansion.

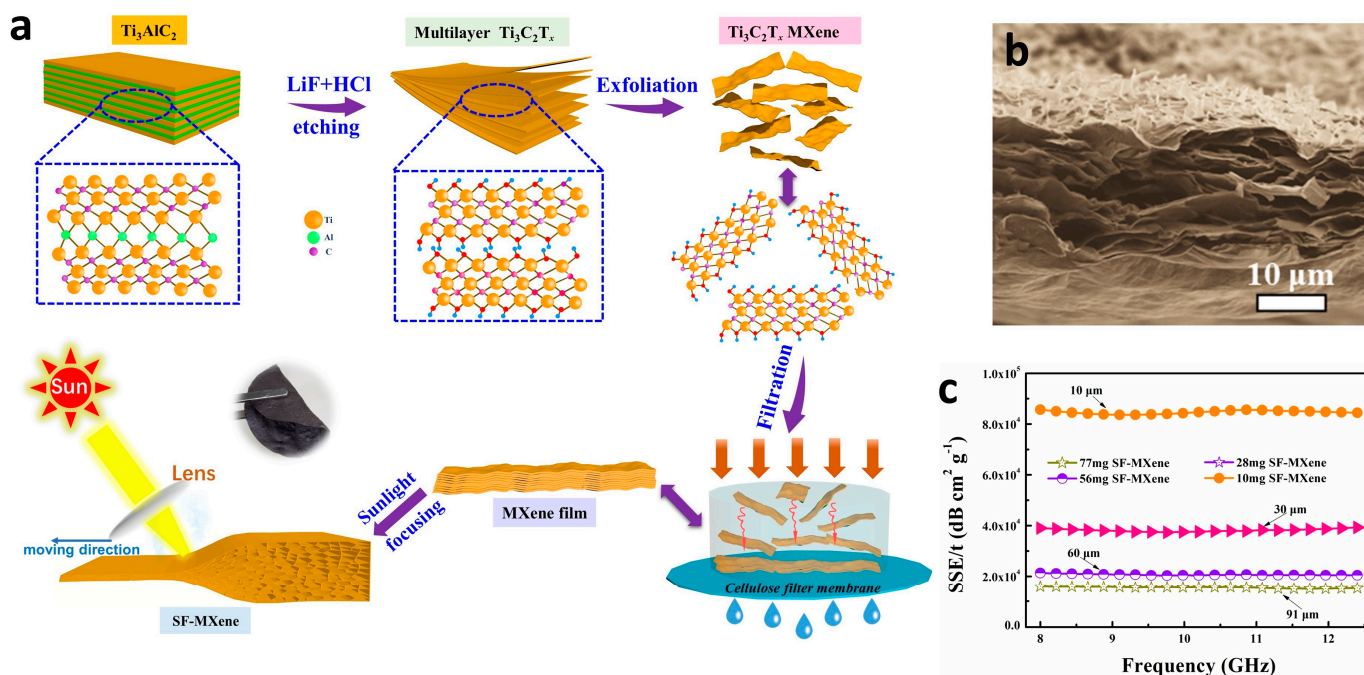


**Figure 16.** (a) Schematic diagram of 3D porous MXene film (SF-MXene) synthesis using focused sunlight. (b) Cross-sectional SEM image of SF-MXene. (c) SSE/ $t$  values of SF-MXene with different thicknesses; reproduced from [62], with the permission of Elsevier.

### 3. Summary and Outlook

Since the synthesis of  $\text{Ti}_3\text{C}_2\text{T}_x$  MXene in 2011, MXenes, a new type of 2D material, has undergone rapid development for more than ten years and has shown potential applications in almost every field. In particular, MXene such as  $\text{Ti}_3\text{C}_2\text{T}_x$ , based on its high conductivity, active terminal functional groups, and good stability, is currently the most widely studied and is most likely to take the lead in realizing the transition from laboratory to industrial applications. Due to the extremely compact structure of the MXene film, directly assembled by MXene ( $\text{Ti}_3\text{C}_2\text{T}_x$ ) nanosheets, its interlayer lacks continuous pore channels for fast ion transport. In addition, the close stacking between the MXene nanosheets significantly reduces the interface, with which the electromagnetic wave can undergo multiple electromagnetic wave attenuations. Therefore, scientists have successfully constructed a series of 3D porous MXene film using the sacrificial template method, vapor foaming method, and light foaming method, exhibiting extremely excellent EMI shielding (Table 1) and electrochemical capacitance storage (Table 2) properties.

**Table 1.** Comparison of EMI shielding performance for typical porous materials.

Materials	Thickness (mm)	EMI SE (dB)	SSE/t (dB cm <sup>2</sup> g <sup>-1</sup> )	SSE (dB cm <sup>3</sup> g <sup>-1</sup> )	Refs
Carbon foam	2	40	1250	241	[63]
Graphene aerogel	3	37	1763	529	[64]
CNT sponge	2.4	22	4621	1100	[65]
Graphene foam	0.3	25.2	13,889	417	[55]
MXene foam	0.06	70	53,030	318	[56]
MXene/rGO foam	1	20.1	4369	43,690	[6]
Porous MXene film	0.085	51	53,058.8	451	[24]
MXene/Calcium Alginate Aerogel film	0.026	54.3	17,586	40.2	[66]
Sunlight Foamed Porous MXene film	0.01	53	88,333	88.3	[62]
MXene/rGO Porous film	0.06	59	37,619	/	[57]
3D Cellular MXene film	0.024	55	127,083	305	[46]

**Table 2.** Comparison of capacitance for some typical MXene electrodes and 3D porous MXene film.

Electrode Materials	Scan Rate	Cg (F g <sup>-1</sup> )	Scan Rate	Cg (F g <sup>-1</sup> )	Refs
MXene	2 mV s <sup>-1</sup>	325	100 mV s <sup>-1</sup>	137.5	[67]
MXene clay	2 mV s <sup>-1</sup>	245	100 mV s <sup>-1</sup>	204	[28]
MXene/PPy	5 mV s <sup>-1</sup>	416	100 mV s <sup>-1</sup>	200	[68]
MXene/MnO <sub>2</sub>	5 mV s <sup>-1</sup>	130	200 mV s <sup>-1</sup>	108	[69]
3D MXene hydrogel	2 mV s <sup>-1</sup>	272	1000 mV s <sup>-1</sup>	226	[70]
3D MXene film	1 A g <sup>-1</sup>	327	20 A g <sup>-1</sup>	199.5	[45]
3D Cellular MXene film	2 mV s <sup>-1</sup>	460	500 mV s <sup>-1</sup>	324	[46]
3D Porous MXene film	20 mV s <sup>-1</sup>	358.8	10,000 mV s <sup>-1</sup>	210.3	[47]
3D Porous MXene/CNTs film	5 mV s <sup>-1</sup>	375	1000 mV s <sup>-1</sup>	251.2	[48]
Nanoporous MXene film	0.5 A g <sup>-1</sup>	346	20 A g <sup>-1</sup>	250.8	[51]
Sunlight foamed porous MXene film	10 mV s <sup>-1</sup>	380	200 mV s <sup>-1</sup>	273	[62]

Sacrificial template method can well design and customize the interlayer pore structure of 3D porous MXene films, but the operation steps are cumbersome and may be detrimental to the intrinsically superior physicochemical properties of MXene materials. The light foaming method has the advantages of simplicity, efficiency, environmental protection, low cost, and easy expansion, but the size of the pore structure is not easy to control. In the future, the sacrificial template method, vapor foaming method, and light foaming method should be combined to give full play to their respective advantages and further develop new foaming processes with high efficiency and customizable interlayer pores. At present, the mainstream MXene synthesis method is, still, to use hydrofluoric acid or generate hydrofluoric acid in situ for etching, so it is potentially dangerous to the human body, and a large amount of waste acid waste liquid is generated, which is not conducive to environmental protection. In addition, since the quality and yield of MXene [71] directly affect the development of subsequent 3D porous MXene films; therefore, continuing to explore green, environmentally friendly, and efficient preparation of antioxidant MXene dispersions is, also, an urgent problem to be solved in the future.

Although 3D porosity is a desirable structural feature of MXene films in the fields of electrochemical energy storage and EMI shielding, it does not necessarily mean that the structure is suitable for both applications. We should get out of this misunderstanding and carry out independent structural design, specifically for these two uses in the future. In

the field of EMI shielding applications, we must increase the pore structure as much as possible on the premise of ensuring the mechanical properties of 3D porous MXene films, since the lightweight properties are more critical for aerospace EMI shielding materials. In the field of electrochemical energy storage, we should reduce the pore structure to the nanometer scale as much as possible, so as to avoid the disadvantage of ineffective electrolyte increasing the overall quality of the device.

**Author Contributions:** Conceptualization, investigation, writing—original draft, H.M.; investigation, C.L.; investigation and supervision, Y.Y.; conceptualization, investigation, supervision, funding acquisition, writing—review, and editing, Z.F. All authors have read and agreed to the published version of the manuscript.

**Funding:** This work was supported by the China Postdoctoral Science Foundation (Grant No. 2019M661274), and the Heilongjiang Postdoctoral Fund (Grant No. LBH-Z19140).

**Institutional Review Board Statement:** Not applicable.

**Informed Consent Statement:** Not applicable.

**Data Availability Statement:** Not applicable.

**Conflicts of Interest:** The authors declare no conflict of interest.

## References

1. Naguib, M.; Kurtoglu, M.; Presser, V.; Lu, J.; Niu, J.; Heon, M.; Hultman, L.; Gogotsi, Y.; Barsoum, M.W. Two-Dimensional Nanocrystals Produced by Exfoliation of  $\text{Ti}_3\text{AlC}_2$ . *Adv. Mater.* **2011**, *23*, 4248–4253. [[CrossRef](#)] [[PubMed](#)]
2. Anasori, B.; Lukatskaya, M.R.; Gogotsi, Y. 2D Metal Carbides and Nitrides (MXenes) for Energy Storage. *Nat. Rev. Mater.* **2017**, *2*, 16098. [[CrossRef](#)]
3. Fan, Z.; Wang, Y.; Xie, Z.; Wang, D.; Yuan, Y.; Kang, H.; Su, B.; Cheng, Z.; Liu, Y. Modified MXene/Holey Graphene Films for Advanced Supercapacitor Electrodes with Superior Energy Storage. *Adv. Sci.* **2018**, *5*, 1800750. [[CrossRef](#)] [[PubMed](#)]
4. Iqbal, A.; Shahzad, F.; Hantanasirisakul, K.; Kim, M.-K.; Kwon, J.; Hong, J.; Kim, H.; Kim, D.; Gogotsi, Y.; Koo, C.M. Anomalous Absorption of Electromagnetic Waves by 2D Transition Metal Carbonitride  $\text{Ti}_3\text{CNT}_x$  (MXene). *Science* **2020**, *369*, 446–450. [[CrossRef](#)]
5. Shahzad, F.; Alhabeb, M.; Hatter, C.B.; Anasori, B.; Hong, S.M.; Koo, C.M.; Gogotsi, Y. Electromagnetic Interference Shielding with 2D Transition Metal Carbides (MXenes). *Science* **2016**, *353*, 1137–1140. [[CrossRef](#)]
6. Fan, Z.; Wang, D.; Yuan, Y.; Wang, Y.; Cheng, Z.; Liu, Y.; Xie, Z. A Lightweight and Conductive MXene/Graphene Hybrid Foam for Superior Electromagnetic Interference Shielding. *Chem. Eng. J.* **2020**, *381*, 122696. [[CrossRef](#)]
7. Zeng, Z.; Wang, C.; Siqueira, G.; Han, D.; Huch, A.; Abdolhosseinzadeh, S.; Heier, J.; Nüesch, F.; Zhag, C.; Nyström, G. Nanocellulose-MXene Biomimetic Aerogels with Orientation-Tunable Electromagnetic Interference Shielding Performance. *Adv. Sci.* **2020**, *7*, 2000979. [[CrossRef](#)]
8. Uzun, S.; Han, M.; Strobel, C.J.; Hantanasirisakul, K.; Goad, A.; Dion, G.; Gogotsi, Y. Highly Conductive and Scalable  $\text{Ti}_3\text{C}_2\text{T}_x$ -Coated Fabrics for Efficient Electromagnetic Interference Shielding. *Carbon* **2021**, *174*, 382–389. [[CrossRef](#)]
9. Lin, H.; Chen, Y.; Shi, J. Insights into 2D MXenes for Versatile Biomedical Applications: Current Advances and Challenges Ahead. *Adv. Sci.* **2018**, *5*, 1800518. [[CrossRef](#)]
10. Wang, L.; Wang, D.; Wang, K.; Jiang, K.; Shen, G. Biocompatible MXene/Chitosan-Based Flexible Bimodal Devices for Real-Time Pulse and Respiratory Rate Monitoring. *ACS Mater. Lett.* **2021**, *3*, 921–929. [[CrossRef](#)]
11. Sarycheva, A.; Polemi, A.; Liu, Y.; Dandekar, K.; Anasori, B.; Gogotsi, Y. 2D Titanium Carbide (MXene) for Wireless Communication. *Sci. Adv.* **2018**, *4*, eaau0920. [[CrossRef](#)] [[PubMed](#)]
12. Li, R.; Zhang, L.; Shi, L.; Wang, P. MXene  $\text{Ti}_3\text{C}_2$ : An Effective 2D Light-to-Heat Conversion Material. *ACS Nano* **2017**, *11*, 3752–3759. [[CrossRef](#)] [[PubMed](#)]
13. Wang, J.; Liu, Y.; Cheng, Z.; Xie, Z.; Yin, L.; Wang, W.; Song, Y.; Zhang, H.; Wang, Y.; Fan, Z. Highly Conductive MXene Film Actuator Based on Moisture Gradients. *Angew. Chem. Int. Ed.* **2020**, *59*, 14029–14033. [[CrossRef](#)] [[PubMed](#)]
14. Wang, J.; Ma, H.; Liu, Y.; Xie, Z.; Fan, Z. MXene-Based Humidity-Responsive Actuators: Preparation and Properties. *ChemPlusChem* **2021**, *86*, 406–417. [[CrossRef](#)] [[PubMed](#)]
15. Jia, G.; Zheng, A.; Wang, X.; Zhang, L.; Li, L.; Li, C.; Zhang, Y.; Cao, L. Flexible, Biocompatible and Highly Conductive MXene-Graphene Oxide Film for Smart Actuator and Humidity Sensor. *Sens. Actuat. B-Chem.* **2021**, *346*, 130507. [[CrossRef](#)]
16. Wang, L.; Qiu, H.; Song, P.; Zhang, Y.; Lu, Y.; Liang, C.; Kong, J.; Chen, L.; Gu, J. 3D  $\text{Ti}_3\text{C}_2\text{T}_x$  MXene/C Hybrid Foam/Epoxy Nanocomposites with Superior Electromagnetic Interference Shielding Performances and Robust Mechanical Properties. *Compos. Part A-Appl. S.* **2019**, *123*, 293–300. [[CrossRef](#)]
17. Cui, Z.; Gao, C.; Fan, Z.; Wang, J.; Cheng, Z.; Xie, Z.; Liu, Y.; Wang, Y. Lightweight MXene/Cellulose Nanofiber Composite Film for Electromagnetic Interference Shielding. *J. Electron. Mater.* **2021**, *50*, 2101–2110. [[CrossRef](#)]

18. Zhan, Z.; Song, Q.; Zhou, Z.; Lu, C. Ultrastrong and Conductive MXene/Cellulose Nanofiber Films Enhanced by Hierarchical Nano-Architecture and Interfacial Interaction for Flexible Electromagnetic Interference Shielding. *J. Mater. Chem. C* **2019**, *7*, 9820–9829. [[CrossRef](#)]
19. Gogotsi, Y.; Anasori, B. The Rise of MXenes. *ACS Nano* **2019**, *13*, 8491–8494. [[CrossRef](#)]
20. Mathis, T.S.; Maleski, K.; Goad, A.; Sarycheva, A.; Anayee, M.; Foucher, A.C.; Hantanasirisakul, K.; Shuck, C.E.; Stach, E.A.; Gogotsi, Y. Modified MAX Phase Synthesis for Environmentally Stable and Highly Conductive  $Ti_3C_2$  MXene. *ACS Nano* **2021**, *15*, 6420–6429. [[CrossRef](#)]
21. Lukatskaya, M.R.; Kota, S.; Lin, Z.; Zhao, M.-Q.; Shpigel, N.; Levi, M.D.; Halim, J.; Taberna, P.-L.; Barsoum, M.W.; Simon, P. Ultra-High-Rate Pseudocapacitive Energy Storage in Two-Dimensional Transition Metal Carbides. *Nat. Energy* **2017**, *2*, 17105. [[CrossRef](#)]
22. Zhang, J.; Kong, N.; Uzun, S.; Levitt, A.; Seyedin, S.; Lynch, P.A.; Qin, S.; Han, M.; Yang, W.; Liu, J. Scalable Manufacturing of Free-Standing, Strong  $Ti_3C_2T_x$  MXene Films with Outstanding Conductivity. *Adv. Mater.* **2020**, *32*, 2001093. [[CrossRef](#)] [[PubMed](#)]
23. Wu, Z.; Shang, T.; Deng, Y.; Tao, Y.; Yang, Q.H. The Assembly of MXenes from 2D to 3D. *Adv. Sci.* **2020**, *7*, 1903077. [[CrossRef](#)] [[PubMed](#)]
24. Lin, Z.; Liu, J.; Peng, W.; Zhu, Y.; Zhao, Y.; Jiang, K.; Peng, M.; Tan, Y. Highly Stable 3D  $Ti_3C_2T_x$  MXene-Based Foam Architectures toward High-Performance Terahertz Radiation Shielding. *ACS Nano* **2020**, *14*, 2109–2117. [[CrossRef](#)] [[PubMed](#)]
25. Bian, R.; He, G.; Zhi, W.; Xiang, S.; Wang, T.; Cai, D. Ultralight MXene-Based Aerogels with High Electromagnetic Interference Shielding Performance. *J. Mater. Chem. C* **2019**, *7*, 474–478. [[CrossRef](#)]
26. Naguib, M.; Barsoum, M.W.; Gogotsi, Y. Ten Years of Progress in the Synthesis and Development of MXenes. *Adv. Mater.* **2021**, *33*, 2103393. [[CrossRef](#)] [[PubMed](#)]
27. Mashtalir, O.; Naguib, M.; Mochalin, V.N.; Dall’Agnese, Y.; Heon, M.; Barsoum, M.W.; Gogotsi, Y. Intercalation and Delamination of Layered Carbides and Carbonitrides. *Nat. Commun.* **2013**, *4*, 1716. [[CrossRef](#)]
28. Ghidui, M.; Lukatskaya, M.R.; Zhao, M.-Q.; Gogotsi, Y.; Barsoum, M.W. Conductive Two-Dimensional Titanium Carbide ‘Clay’ with High Volumetric Capacitance. *Nature* **2014**, *516*, 78–81. [[CrossRef](#)]
29. Alhabeab, M.; Maleski, K.; Anasori, B.; Lelyukh, P.; Clark, L.; Sin, S.; Gogotsi, Y. Guidelines for Synthesis and Processing of Two-Dimensional Titanium Carbide ( $Ti_3C_2T_x$  MXene). *Chem. Mater.* **2017**, *29*, 7633–7644. [[CrossRef](#)]
30. Lipatov, A.; Alhabeab, M.; Lukatskaya, M.R.; Boson, A.; Gogotsi, Y.; Sinitskii, A. Effect of Synthesis on Quality, Electronic Properties and Environmental Stability of Individual Monolayer  $Ti_3C_2$  MXene Flakes. *Adv. Electron. Mater.* **2016**, *2*, 1600255. [[CrossRef](#)]
31. Zhao, X.; Vashisth, A.; Prehn, E.; Sun, W.; Shah, S.A.; Habib, T.; Chen, Y.; Tan, Z.; Lutkenhaus, J.L.; Radovic, M. Antioxidants Unlock Shelf-Stable  $Ti_3C_2T_x$  (MXene) Nanosheet Dispersions. *Matter* **2019**, *1*, 513–526. [[CrossRef](#)]
32. Fan, Z.; He, H.; Yu, J.; Wang, J.; Yin, L.; Cheng, Z.; Xie, Z.; Wang, Y.; Liu, Y. Binder-Free  $Ti_3C_2T_x$  MXene Doughs with High Redispersibility. *ACS Mater. Lett.* **2020**, *2*, 1598–1605. [[CrossRef](#)]
33. Natu, V.; Hart, J.L.; Sokol, M.; Chiang, H.; Taheri, M.L.; Barsoum, M.W. Edge Capping of 2D-MXene Sheets with Polyanionic Salts To Mitigate Oxidation in Aqueous Colloidal Suspensions. *Angew. Chem. Int. Ed.* **2019**, *58*, 12655–12660. [[CrossRef](#)]
34. Shuck, C.E.; Sarycheva, A.; Anayee, M.; Levitt, A.; Zhu, Y.; Uzun, S.; Balitskiy, V.; Zahorodna, V.; Gogotsi, O.; Gogotsi, Y. Scalable Synthesis of  $Ti_3C_2T_x$  MXene. *Adv. Eng. Mater.* **2020**, *22*, 1901241. [[CrossRef](#)]
35. Shuck, C.E.; Gogotsi, Y. Taking MXenes from the Lab to Commercial Products. *Chem. Eng. J.* **2020**, *401*, 125786. [[CrossRef](#)]
36. Jiang, Y.; Wang, Y.; Xu, Z.; Gao, C. Conformation Engineering of Two-Dimensional Macromolecules: A Case Study with Graphene Oxide. *Acc. Mater. Res.* **2020**, *1*, 175–187. [[CrossRef](#)]
37. Shao, H.; Xu, K.; Wu, Y.-C.; Iadecola, A.; Liu, L.; Ma, H.; Qu, L.; Raymundo-Piñero, E.; Zhu, J.; Lin, Z. Unraveling the Charge Storage Mechanism of  $Ti_3C_2T_x$  MXene Electrode in Acidic Electrolyte. *ACS Energy Lett.* **2020**, *5*, 2873–2880. [[CrossRef](#)]
38. Fan, Z.; Wang, J.; Kang, H.; Wang, Y.; Xie, Z.; Cheng, Z.; Liu, Y. A Compact MXene Film with Folded Structure for Advanced Supercapacitor Electrode Material. *ACS Appl. Energy Mater.* **2020**, *3*, 1811–1820. [[CrossRef](#)]
39. Huang, X.; Huang, J.; Yang, D.; Wu, P. A Multi-Scale Structural Engineering Strategy for High-Performance MXene Hydrogel Supercapacitor Electrode. *Adv. Sci.* **2021**, *8*, 2101664. [[CrossRef](#)]
40. Xia, Y.; Mathis, T.S.; Zhao, M.-Q.; Anasori, B.; Dang, A.; Zhou, Z.; Cho, H.; Gogotsi, Y.; Yang, S. Thickness-Independent Capacitance of Vertically Aligned Liquid-Crystalline MXenes. *Nature* **2018**, *557*, 409–412. [[CrossRef](#)]
41. Hu, M.; Cheng, R.; Li, Z.; Hu, T.; Zhang, H.; Shi, C.; Yang, J.; Cui, C.; Zhang, C.; Wang, H.; et al. Interlayer Engineering of  $Ti_3C_2T_x$  MXenes towards High Capacitance Supercapacitors. *Nanoscale* **2020**, *12*, 763–771. [[CrossRef](#)] [[PubMed](#)]
42. Wang, J.; Kang, H.; Ma, H.; Liu, Y.; Xie, Z.; Wang, Y.; Fan, Z. Super-Fast Fabrication of MXene Film through a Combination of Ion Induced Gelation and Vacuum-Assisted Filtration. *Eng. Sci.* **2021**, *15*, 57–66. [[CrossRef](#)]
43. Lipton, J.; Röhr, J.A.; Dang, V.; Goad, A.; Maleski, K.; Lavini, F.; Han, M.; Tsai, E.H.; Weng, G.-M.; Kong, J. Scalable, Highly Conductive, and Micropatternable MXene Films for Enhanced Electromagnetic Interference Shielding. *Matter* **2020**, *3*, 546–557. [[CrossRef](#)]
44. Wang, J.; Liu, Y.; Yang, Y.; Wang, J.; Kang, H.; Yang, H.; Zhang, D.; Cheng, Z.; Xie, Z.; Tan, H.; et al. A Weldable MXene Film Assisted by Water. *Matter* **2022**, *5*, 1042–1055. [[CrossRef](#)]
45. Zhang, X.; Liu, X.; Dong, S.; Yang, J.; Liu, Y. Template-Free Synthesized 3D Macroporous MXene with Superior Performance for Supercapacitors. *Appl. Mater. Today* **2019**, *16*, 315–321. [[CrossRef](#)]

46. Fan, Z.; He, H.; Yu, J.; Liu, L.; Liu, Y.; Xie, Z. Lightweight Three-Dimensional Cellular MXene Film for Superior Energy Storage and Electromagnetic Interference Shielding. *ACS Appl. Energy Mater.* **2020**, *3*, 8171–8178. [[CrossRef](#)]
47. Kong, J.; Yang, H.; Guo, X.; Yang, S.; Huang, Z.; Lu, X.; Bo, Z.; Yan, J.; Cen, K.; Ostrikov, K.K. High-Mass-Loading Porous  $\text{Ti}_3\text{C}_2\text{T}_x$  Films for Ultrahigh-Rate Pseudocapacitors. *ACS Energy Lett.* **2020**, *5*, 2266–2274. [[CrossRef](#)]
48. Zhang, P.; Zhu, Q.; Soomro, R.A.; He, S.; Sun, N.; Qiao, N.; Xu, B. In Situ Ice Template Approach to Fabricate 3D Flexible MXene Film-Based Electrode for High Performance Supercapacitors. *Adv. Funct. Mater.* **2020**, *30*, 2000922. [[CrossRef](#)]
49. Zhao, M.Q.; Xie, X.; Ren, C.E.; Makaryan, T.; Anasori, B.; Wang, G.; Gogotsi, Y. Hollow MXene Spheres and 3D Macroporous MXene Frameworks for Na-Ion Storage. *Adv. Mater.* **2017**, *29*, 1702410. [[CrossRef](#)]
50. Zhao, Q.; Zhu, Q.; Miao, J.; Zhang, P.; Wan, P.; He, L.; Xu, B. Flexible 3D Porous MXene Foam for High-Performance Lithium-Ion Batteries. *Small* **2019**, *15*, 1904293. [[CrossRef](#)]
51. Fan, Z.; Wang, Y.; Xie, Z.; Xu, X.; Yuan, Y.; Cheng, Z.; Liu, Y. A Nanoporous MXene Film Enables Flexible Supercapacitors with High Energy Storage. *Nanoscale* **2018**, *10*, 9642–9652. [[CrossRef](#)] [[PubMed](#)]
52. Tang, J.; Mathis, T.; Zhong, X.; Xiao, X.; Wang, H.; Anayee, M.; Pan, F.; Xu, B.; Gogotsi, Y. Optimizing Ion Pathway in Titanium Carbide MXene for Practical High-Rate Supercapacitor. *Adv. Energy Mater.* **2021**, *11*, 2003025. [[CrossRef](#)]
53. Fan, Z.; Yang, Y.; Ma, H.; Wang, Y.; Xie, Z.; Liu, Y. High-Volumetric Capacitance and High-Rate Performance in Liquid-Mediated Densified Holey MXene Film. *Carbon* **2022**, *186*, 150–159. [[CrossRef](#)]
54. Niu, Z.; Chen, J.; Hng, H.H.; Ma, J.; Chen, X. A Leavening Strategy to Prepare Reduced Graphene Oxide Foams. *Adv. Mater.* **2012**, *24*, 4144–4150. [[CrossRef](#)] [[PubMed](#)]
55. Shen, B.; Li, Y.; Yi, D.; Zhai, W.; Wei, X.; Zheng, W. Microcellular Graphene Foam for Improved Broadband Electromagnetic Interference Shielding. *Carbon* **2016**, *102*, 154–160. [[CrossRef](#)]
56. Liu, J.; Zhang, H.B.; Sun, R.; Liu, Y.; Liu, Z.; Zhou, A.; Yu, Z.Z. Hydrophobic, Flexible, and Lightweight MXene Foams for High-Performance Electromagnetic-Interference Shielding. *Adv. Mater.* **2017**, *29*, 1702367. [[CrossRef](#)]
57. Zhang, Y.; Ruan, K.; Shi, X.; Qiu, H.; Pan, Y.; Yan, Y.; Gu, J.  $\text{Ti}_3\text{C}_2\text{T}_x/\text{rGO}$  Porous Composite Films with Superior Electromagnetic Interference Shielding Performances. *Carbon* **2021**, *175*, 271–280. [[CrossRef](#)]
58. Li, Z.; Zhang, H.; Han, J.; Chen, Y.; Lin, H.; Yang, T. Surface Nanopore Engineering of 2D MXenes for Targeted and Synergistic Multitherapies of Hepatocellular Carcinoma. *Adv. Mater.* **2018**, *30*, 1706981. [[CrossRef](#)]
59. Lin, H.; Wang, X.; Yu, L.; Chen, Y.; Shi, J. Two-Dimensional Ultrathin MXene Ceramic Nanosheets for Photothermal Conversion. *Nano Lett.* **2017**, *17*, 384–391. [[CrossRef](#)]
60. Ding, L.; Li, L.; Liu, Y.; Wu, Y.; Lu, Z.; Deng, J.; Wei, Y.; Caro, J.; Wang, H. Effective Ion sieving with  $\text{Ti}_3\text{C}_2\text{T}_x$  MXene Membranes for Production of Drinking Water from Seawater. *Nat. Sustain.* **2020**, *3*, 296–302. [[CrossRef](#)]
61. Tang, J.; Yi, W.; Zhong, X.; Zhang, C.J.; Xiao, X.; Pan, F.; Xu, B. Laser Writing of the Restacked Titanium Carbide MXene for High Performance Supercapacitors. *Energy Storage Mater.* **2020**, *32*, 418–424. [[CrossRef](#)]
62. Yin, L.; Kang, H.; Ma, H.; Wang, J.; Liu, Y.; Xie, Z.; Wang, Y.; Fan, Z. Sunshine Foaming of Compact  $\text{Ti}_3\text{C}_2\text{T}_x$  MXene Film for Highly Efficient Electromagnetic Interference Shielding and Energy Storage. *Carbon* **2021**, *182*, 124–133. [[CrossRef](#)]
63. Moglie, F.; Micheli, D.; Laurenzi, S.; Marchetti, M.; Primiani, V.M. Electromagnetic Shielding Performance of Carbon Foams. *Carbon* **2012**, *50*, 1972–1980. [[CrossRef](#)]
64. Song, W.L.; Guan, X.T.; Fan, L.Z.; Cao, W.Q.; Wang, C.Y.; Cao, M.S. Tuning Three-Dimensional Textures with Graphene Aerogels for Ultra-Light Flexible Graphene/Texture Composites of Effective Electromagnetic Shielding. *Carbon* **2015**, *93*, 151–160. [[CrossRef](#)]
65. Crespo, M.; González, M.; Elías, A.L.; Pulickal Rajukumar, L.; Baselga, J.; Terrones, M.; Pozuelo, J. Ultra-Light Carbon Nanotube Sponge as an Efficient Electromagnetic Shielding Material in the GHz Range. *Phys. Status Solidi RRL* **2014**, *8*, 698–704. [[CrossRef](#)]
66. Zhou, Z.; Liu, J.; Zhang, X.; Tian, D.; Zhan, Z.; Lu, C. Ultrathin MXene/Calcium Alginate Aerogel Film for High-Performance Electromagnetic Interference Shielding. *Adv. Mater. Interfaces* **2019**, *6*, 1802040. [[CrossRef](#)]
67. Dall’Agnese, Y.; Lukatskaya, M.R.; Cook, K.M.; Taberna, P.-L.; Gogotsi, Y.; Simon, P. High Capacitance of Surface-Modified 2D Titanium Carbide in Acidic Electrolyte. *Electrochem. Commun.* **2014**, *48*, 118–122. [[CrossRef](#)]
68. Boota, M.; Anasori, B.; Voigt, C.; Zhao, M.-Q.; Barsoum, M.W.; Gogotsi, Y. Pseudocapacitive Electrodes Produced by Oxidant-Free Polymerization of Pyrrole between the Layers of 2D Titanium Carbide (MXene). *Adv. Mater.* **2016**, *28*, 1517–1522. [[CrossRef](#)]
69. Tang, Y.; Zhu, J.; Yang, C.; Wang, F. Enhanced Supercapacitive Performance of Manganese Oxides Doped Two-Dimensional Titanium Carbide Nanocomposite in Alkaline Electrolyte. *J. Alloys Compd.* **2016**, *685*, 194–201. [[CrossRef](#)]
70. Deng, Y.; Shang, T.; Wu, Z.; Tao, Y.; Luo, C.; Liang, J.; Han, D.; Lyu, R.; Qi, C.; Lv, W. Fast Gelation of  $\text{Ti}_3\text{C}_2\text{T}_x$  MXene Initiated by Metal Ions. *Adv. Mater.* **2019**, *31*, 1902432. [[CrossRef](#)]
71. Shekhirev, M.; Shuck, C.E.; Sarycheva, A.; Gogotsi, Y. Characterization of MXenes at Every Step, from Their Precursors to Single Flakes and Assembled Films. *Prog. Mater. Sci.* **2021**, *120*, 100757. [[CrossRef](#)]